

Brillouin light scattering study of $\text{Co}_2\text{Cr}_{0.6}\text{Fe}_{0.4}\text{Al}$ and Co_2FeAl Heusler compounds

O. Gaier*, J. Hamrle, S. Trudel, A. Conca Parra, B. Hillebrands

Fachbereich Physik and Forschungsschwerpunkt OPTIMAS,

Technische Universität Kaiserslautern,

Erwin-Schrödinger-Straße 56, D-67663 Kaiserslautern, Germany

E. Arbelo, C. Herbort, M. Jourdan

Institut für Physik, Johannes-Gutenberg-Universität Mainz,

Staudinger Weg 7, D-55099 Mainz, Germany

Abstract

The thermal magnonic spectra of $\text{Co}_2\text{Cr}_{0.6}\text{Fe}_{0.4}\text{Al}$ (CCFA) and Co_2FeAl were investigated using Brillouin light scattering spectroscopy (BLS). For CCFA, the exchange constant A (exchange stiffness D) is found to be $0.48 \pm 0.04 \mu\text{erg}/\text{cm}$ ($203 \pm 16 \text{ meV } \text{Å}^2$), while for Co_2FeAl the corresponding values of $1.55 \pm 0.05 \mu\text{erg}/\text{cm}$ ($370 \pm 10 \text{ meV } \text{Å}^2$) were found. The observed asymmetry in the BLS spectra between the Stokes and anti-Stokes frequencies was assigned to an interplay between the asymmetrical profiles of hybridized Damon-Esbach and perpendicular standing spin-wave modes, combined with the optical sensitivity of the BLS signal to the upper side of the CCFA or Co_2FeAl film.

PACS numbers: 75.30.Et, 78.35.+c, 75.30.Ds, 75.50.Cc

* Corresponding author: email: gaier@physik.uni-kl.de

I. INTRODUCTION

Studies of ferromagnetic (FM) half-metals are mainly driven by the possible applications of such materials in spintronic devices as a potential source of a 100% polarized spin current. Some Heusler alloys are promising candidates due to their high Curie temperatures [1]. For example, it was recently proven that spin injection from Co_2FeSi into the semiconductor $(\text{Al,Ga})\text{As}$ can be achieved with a 50% efficiency [2].

Amongst the different Heusler systems studied in recent years, the compound $\text{Co}_2\text{Cr}_{0.6}\text{Fe}_{0.4}\text{Al}$ (CCFA) has attracted significant experimental [3, 4, 5, 6, 7, 8] and theoretical [9, 10, 11] attention. CCFA is an interesting candidate for spintronics applications due to its high Curie temperature of 760 K [3] and its high value of volume magnetization of $\approx 3\mu_B$ per formula unit [5, 12] at 5 K (the theoretical value is $3.8\mu_B$ per formula unit [13]). Using spin resolved photoemission, the spin polarization of CCFA at the Fermi level was found to be 45% at room temperature [14]. CCFA-based spin-dependent transport devices showing large magnetoresistance effects were recently reported. For example, in the simple CCFA/Cu/ $\text{Co}_{90}\text{Fe}_{10}$ trilayers a large giant magnetoresistance of 6.8% at room temperature (RT) [15] was found. Tunnelling magnetoresistance ratios (TMR) of 52% at RT and 83% at 5K were reported for the CCFA/ AlO_x / $\text{Co}_{75}\text{Fe}_{25}$ magnetic tunnel junction (MTJ) [12]. In the epitaxial CCFA/MgO/ $\text{Co}_{50}\text{Fe}_{50}$ MTJ structure, TMR ratios of 109% at RT and 317% at 4.2 K [16] were presented, whereas for the epitaxial CCFA/MgO/CCFA structure TMR ratios of 60% at RT and 238% at 4.2 K are reported [17].

Thin Co_2FeAl films and MTJ structures containing the Co_2FeAl electrode have been a subject of extensive studies as well [12, 18, 19, 20, 21], even though initial band structure calculations predicted a much lower degree of spin polarization compared to CCFA [9]. However, recent band structure calculations by Felser *et al.* have predicted 100% spin polarization at the Fermi level for bulk Co_2FeAl [11, 22]. The TMR ratios reported in Refs. [12, 18, 19, 20, 21] are about 50% at room temperature and are comparable to those reported for CCFA.

In this article we report on our study of the thermal spectrum of spin waves in CCFA and Co_2FeAl films using Brillouin light scattering (BLS) spectroscopy. From our BLS spectra we have determined the values of the exchange constants for CCFA and Co_2FeAl .

II. SAMPLE PREPARATION AND CHARACTERIZATION

The CCFA structure under investigation is an Al(2.5nm)/CCFA(80nm)/Cr(8nm)/-MgO(100) epitaxial structure [5, 23]. The buffer layers were deposited by electron beam evaporation onto a single-crystalline MgO(001) substrate, while the epitaxial CCFA films were subsequently deposited by dc magnetron sputtering. A more detailed description of the sample preparation can be found elsewhere [5]. The films grow with the B2 structure, as there is full disorder between the Cr and Al positions, but order on the Co positions [5]. A volume magnetization of $\mu_{\text{CCFA}} \approx 2.5\mu_B$ per f.u. (formula unit) (i.e. $M_s = 490 \text{ emu/cm}^3$) was measured at 300 K by SQUID magnetometry. 4-circle x-ray diffraction (XRD) scans yielded lattice parameters $a = 0.570 \pm 0.005 \text{ nm}$ and $b = c = 0.583 \pm 0.012 \text{ nm}$, where the a -axis is perpendicular to the sample surface, and b and c are in-plane axes [23]. The magnetic reversal of the structure is also described in Ref. [23].

The Co_2FeAl sample under investigation consists of an 80 nm thick Co_2FeAl layer which was epitaxially grown on a single-crystalline MgO(001) substrate covered with a 10 nm thick MgO buffer layer. Magnetron sputtering was employed for the deposition of both the MgO buffer and the Co_2FeAl layer. A post-growth anneal at 550°C provided a Co_2FeAl film with the B2 structure, as confirmed by XRD measurements. A 3 nm thick AlO_x capping layer was deposited on top of the structure to prevent sample oxidation. The sample exhibits a saturation magnetization of $4.66 \mu_B/\text{f.u.}$ measured by SQUID magnetometry at room temperature. This is in a good agreement with the previously reported value of $4.96 \mu_B/\text{f.u.}$ determined at 4.2 K [24].

All BLS measurements presented in this article were performed using a diode pumped, frequency doubled Nd:YVO₄ laser with a wavelength of $\lambda = 532 \text{ nm}$ as a light source. Unless specified otherwise, the light impinges on the sample at an angle of incidence of $\varphi = 45^\circ$, corresponding to a transferred wave vector of detected magnons $q_{\parallel} = 4\pi/\lambda \sin \varphi = 1.67 \cdot 10^5 \text{ cm}^{-1}$. The external magnetic field H was applied in the so-called magnetostatic surface mode geometry, wherein H is applied in the plane of the sample, and is perpendicular to the plane of light incidence (i.e., $\vec{H} \perp \vec{q}_{\parallel}$). A more detailed description of the BLS setup used in this work can be found in Refs. [25, 26].

III. EXPERIMENTAL RESULTS

A. CCFA

Typical BLS spectra measured on the investigated CCFA film are presented in Fig. 1 for several values of the external magnetic field. As is clearly visible, the positions of the peaks in both the Stokes (creation of magnons, negative frequencies in BLS spectra) and anti-Stokes (annihilation of magnons, positive frequencies in BLS spectra) parts of the spectrum move to higher values with an increasing magnetic field. This field dependence is evidence of the magnonic nature of the observed peaks, whereas the position of a phononic peak is not expected to be field dependent. The observed peaks correspond to the Damon-Eshbach (DE) mode and to the perpendicular standing spin-wave (PSSW) modes. As will be discussed below, one of the observed peaks in the BLS spectra results from the hybridization of the DE and the second PSSW mode. Therefore, this mode will be referred as PSSW2+DE in the following discussion. The other observed peaks are pure PSSW modes.

Figures 2(a,b) provide the dependence of the observed spin wave frequencies on the value of the external magnetic field which was applied along the [110] (Fig. 2(a)) and the [100] (Fig. 2(b)) directions of the CCFA film. The field dependencies are nearly identical for both orientations of the external magnetic field. However, the observed spin wave frequencies are about 1 GHz smaller when H is aligned parallel to the $[100]_{\text{CCFA}}$ direction, compared to when the field is applied along the [110] direction. This is also illustrated in Fig. 2(c), where the dependence of the observed spin wave frequencies on the in-plane sample orientation (i.e., the angle between [100] direction and the applied magnetic field) is presented. The lower frequency observed when the field is along the $[100]_{\text{CCFA}}$ direction indicates that this direction is an in-plane magnetically hard axis [27], in agreement with previous MOKE investigations [23].

The solid lines in Figures 2(a–c) are a fit to the experimental data using a theoretical model described in Ref. [28]. The found parameters are: exchange constant $A = 0.48 \pm 0.04 \mu\text{erg}/\text{cm}$, cubic volume anisotropy $K_1 = -20 \pm 10 \text{ kerg}/\text{cm}^3$, Landé g -factor $g = 1.9 \pm 0.1$ and saturation magnetization $M_S = 520 \pm 20 \text{ emu}/\text{cm}^3$. Note that each of the fitted parameter is determined rather independently by a particular experimental dependence or feature, making the fit reliable and providing results with a relatively small error. Namely,

M_S is obtained from the frequency of the DE mode (here PSSW2+DE mode), and agrees well with the SQUID value $M_S = 490 \text{ emu/cm}^3$ [5]. Landé g -factor is provided by the slope of BLS frequency on the external field. K_1 is determined from the variation of BLS frequencies on the sample orientation (Fig. 2(c)). Finally, the exchange constant A is determined by frequencies of PSSW modes. Note, that the corresponding exchange stiffness of CCFA is $D = 2Ag\gamma_0\hbar/M_S = 203 \pm 16 \text{ meV \AA}^2$, where \hbar and $\gamma = g\gamma_0$ are the reduced Planck constant and the gyromagnetic ratio, respectively.

For the PSSW2+DE mode we observe a large (between 0.5–1 GHz) splitting between the Stokes (\blacktriangle) and the anti-Stokes (\blacktriangledown) frequencies (Figs. 2(a,b)). This splitting is particularly pronounced for small values of the external field in the range of 100–400 Oe. A careful investigation of Figs. 2(a,b) further reveals that the lower frequency component of the split PSSW2+DE mode are observed only in the Stokes part of the BLS spectrum, whereas the higher frequency component appears only in the anti-Stokes part. Moreover, the slope df/dH is slightly different for frequencies determined from the Stokes and anti-Stokes parts of the BLS spectra. In the case of a DE mode, such an asymmetry usually indicates different pinning conditions of the dynamic magnetization on each interface [39]. However, in our particular case, the observed asymmetry is related to the hybridization (also called mode repulsion) of the DE and the PSSW2 modes, which is elaborated in detail in the Discussion section.

B. Co_2FeAl

The BLS spectra collected from the Co_2FeAl sample are shown in Fig. 3. In (a) spectra recorded at a transferred wave vector $q_{\parallel} = 1.67 \cdot 10^5 \text{ cm}^{-1}$ and different values of the external magnetic field are displayed, while in (b) BLS spectra measured at $H = 1 \text{ kOe}$ and at different q_{\parallel} are presented. As is clearly visible from Fig. 3(a), the positions of the peaks move to higher values as the magnetic field increases, confirming the magnonic origin of the observed peaks.

Performing BLS measurements at different angles of incidence φ (i.e. at different values of q_{\parallel}), allows for an unambiguous separation of the dipole dominated magnetostatic surface wave (the Damon-Eshbach mode), from the exchange dominated perpendicular standing spin waves (PSSW). In contrast to PSSW modes, the frequency of the DE mode exhibits

a much stronger dependence on the in-plane direction of the wave vector. Therefore it provides substantial shifts in the collected spectra upon the variation of φ (and thus q_{\parallel}), while the spectral positions of the PSSW modes are not significantly affected by this variation. Therefore the peak originating from the DE mode excitation can be easily identified. (Fig. 3(b)).

The extracted peak positions as a function of external magnetic field and incidence angle are presented by symbols in Fig. 4(a) and (b), respectively. The solid lines present the simulation from which the following parameters were determined: exchange constant $A = 1.55 \pm 0.05 \mu\text{erg}/\text{cm}$, saturation magnetization $M_S = 1027 \pm 10 \text{ emu}/\text{cm}^3$ and Landé g -factor $g = 2.1 \pm 0.1$. The corresponding exchange stiffness is $D = 370 \pm 10 \text{ meV } \text{\AA}^2$. The value of the cubic volume anisotropy K_1 was not determined and hence its value is assumed to be zero in the simulations. Note that including K_1 into the model only slightly changes the frequency of the spin waves (by about 1 GHz). Therefore, setting K_1 to zero in the model used does not detrimentally affect the determination of M_S and A .

Note that in the Stokes part of the spectrum (i.e. negative frequencies) shown in Fig. 3(a), the PSSW2 mode is difficult to recognize. This is due to a relatively small spacing between the PSSW2 and DE modes, as well as the much stronger intensity of the adjacent DE mode. In the anti-Stokes region of the spectrum, the DE mode has intensities that are comparable to, or lesser than the PSSW2 mode. The origin of this asymmetry of the DE mode intensities will be discussed in the following.

IV. DISCUSSION

The values of exchange constant (exchange stiffness) of CCFA was found to be $A = 0.48 \pm 0.04 \mu\text{erg}/\text{cm}$ ($D = 203 \pm 16 \text{ meV } \text{\AA}^2$), whereas the corresponding value for Co_2FeAl was found to be $A = 1.55 \pm 0.05 \mu\text{erg}/\text{cm}$ ($D = 370 \pm 10 \text{ meV } \text{\AA}^2$). This exchange constant found for Co_2FeAl is smaller than both the exchange constants of bcc Fe ($A_{\text{Fe}} = 2.0 \mu\text{erg}/\text{cm}$, $D_{\text{Fe}} = 280 \text{ meV } \text{\AA}^2$ [28, 29, 30]) and of bcc Co ($A_{\text{Co}} = 2.12 \mu\text{erg}/\text{cm}$, $D_{\text{Co}} = 430 \text{ meV } \text{\AA}^2$ [31]). However, the exchange stiffness of Co_2FeAl is between the exchange stiffness of bcc Fe and bcc Co. On the other hand, the value of the exchange constant (exchange stiffness) of CCFA is very small, being only one third (one half) of the exchange constant (exchange stiffness) of Co_2FeAl , and about one half of the exchange constant or exchange stiffness of

fcc Ni ($A_{\text{Ni}} = 0.85 \text{ erg/cm}$, $D_{\text{Ni}} = 420 \text{ meV \AA}^2$). The large discrepancy between the values of exchange determined for Co_2FeAl and CCFA demonstrates how these can vary substantially in Co_2 -based Heusler compounds, even for compounds with the same ordering (B2) and similar compositions.

The value of the cubic volume anisotropy K_1 in CCFA is found to be $-20 \pm 10 \text{ kerg/cm}^3$, being about 24 times smaller than K_1 of bcc Fe ($K_{1,\text{Fe}} = 480 \text{ kerg/cm}^3$ [32]). However, it is roughly of the order of bcc Co ($K_{1,\text{Co}} = 0 \pm 10 \text{ kerg/cm}^3$ [31]). The small value of K_1 in CCFA found here is consistent with previous investigations showing that the magnetic anisotropy is weak in Heusler compounds [33, 34], reflecting the small anisotropy of the spin-orbit coupling in these materials [35].

To explain the aforementioned asymmetries between the Stokes and anti-Stokes peak positions in the BLS spectra, we calculated the depth profiles of the dynamic magnetization for CCFA and Co_2FeAl films, using the model presented in Ref. [28]. The results for CCFA are presented in Fig. 5 for CCFA thicknesses $t = 60$ and 80 nm , along with the calculated dependence of the spin wave frequencies on the CCFA thickness. This figure shows that in the vicinity of $t = 80 \text{ nm}$, i.e. the thickness of the investigated CCFA film, a crossing between the DE and the PSSW modes occurs, resulting in a hybridization of these two modes. Due to the hybridization, a gap of 0.3 GHz is created, which corresponds to the splitting between the Stokes and anti-Stokes frequencies.

The hybridization is also visible in the calculated depth profiles of the dynamic magnetization in Fig. 5. The left part of each profile image shows the trajectories of the magnetization vector along the film depth (the trajectory at a given depth is an ellipse). In the corresponding right part of each image the profiles of the in-plane and out-of-plane components of the dynamic magnetization are shown, denoted by green solid and red dashed lines, respectively. Note that due to the shape anisotropy of the CCFA film, the amplitude of the in-plane dynamic magnetization is roughly twice as large as the amplitude in the out-of plane direction. As demonstrated for $t = 60 \text{ nm}$, the DE mode has a large dynamic magnetization nearby one interface and decays to the second interface. The m -th order mode of the PSSW has m nodes, (i.e., there is m points in the depth of the CCFA film where the dynamic magnetization is zero) and is symmetrical with respect to both interfaces [36]. For the 80 nm thick film, the profiles of both hybridized modes (denoted as DE/PSSW2 and PSSW2/DE) have characteristic features of both types of modes, namely they exhibit a larger dynamic

magnetization nearby one of the interfaces (a characteristic feature of the DE mode) and they support two nodes (a feature of the PSSW2 mode). A careful investigation of those two modes shows that when the maximum dynamic amplitude for the DE/PSSW2 mode is at the upper interface, the PSSW2/DE mode has a larger amplitude at the opposite interface.

The presented depth profiles of the dynamic magnetization shown in Fig. 5 were calculated for the anti-Stokes modes. For the Stokes modes, the profiles are reversed, i.e. modes that were bound to the upper interface are now bound to the bottom interface, and *vice versa*. Since the typical probing depth for the laser wavelength used in our BLS experiments is about 20–30 nm [37, 38], the experiments presented here are only sensitive to the dynamic magnetization nearby the upper interface. Furthermore, the sensitivity to the out-of-plane magnetization component is about twice as large compared to in-plane component in the given geometry ($\varphi = 45^\circ$). Combining these two points with the discussed mode profiles shows that the DE/PSSW2 (PSSW2/DE) mode provides a larger signal in the anti-Stokes (Stokes) part of the BLS spectra. This explains why different spin wave modes are observed in the Stokes and anti-Stokes parts of the BLS spectra of the CCFA film.

There are several analogies between the mode splitting observed in the CCFA film and the BLS spectra observed in the Co_2FeAl film (Fig. 4). (i) The DE and PSSW2 modes observed in the Co_2FeAl are rather close to each other (about 2 GHz) (ii) the DE and PSSW2 mode frequencies have different slopes df/dH . (iii) In the Stokes part of the BLS spectra, only the DE mode is visible, since the BLS intensity of the DE mode is much larger than the BLS intensity of PSSW2 mode. (iv) The dependence of the BLS frequency on the Co_2FeAl thickness (presented in Fig. 6(a)) is similar to that of CCFA (Fig. 5). In particular, the DE and PSWW2 modes cross each other at a thickness of about 80 nm in both cases. (v) The calculated profiles of the dynamic magnetization in Co_2FeAl for the DE and PSSW2 modes (shown in Fig. 6(b)) demonstrate that they are hybridized. Furthermore, the profiles of those modes are very similar to the profiles of hybridized modes at $t = 80$ nm found in the CCFA film (Fig. 5).

Therefore, the BLS intensities of each mode are expected to be similar too, which is indeed observed experimentally. While the DE and PSSW2 waves are indistinguishable in CCFA due to a small difference in frequency between these two modes, the frequency difference between these same two modes is larger in the anti-Stokes part of the BLS spectra for Co_2FeAl , which allowed us to differentiate them. As such, in the case of Co_2FeAl , we can

see that the intensity of the DE mode is smaller than the intensity of the PSSW2 mode on the anti-Stokes side. It confirms our discussion regarding CCFA, showing that the observed mode splitting in CCFA is an interplay between asymmetrical profiles of hybridized modes and the optical depth selectivity of the BLS signal.

V. CONCLUSION

We have investigated thermal spin waves in CCFA and Co₂FeAl using BLS spectroscopy. The values of the exchange constant (exchange stiffness) of CCFA was found to be $A = 0.48 \pm 0.04 \mu\text{erg}/\text{cm}$ ($D = 203 \pm 16 \text{ meV } \text{\AA}^2$) whereas the exchange of Co₂FeAl was found to be $A = 1.55 \pm 0.05 \mu\text{erg}/\text{cm}$ ($D = 370 \pm 10 \text{ meV } \text{\AA}^2$). The found cubic volume magnetic anisotropy of CCFA $K_1 = -20 \pm 10 \text{ kerg}/\text{cm}^3$ is in agreement with small values of K_1 found for other Heusler compounds.

The observed asymmetry in BLS spectra between Stokes and anti-Stokes frequencies was assigned to an interplay between asymmetrical profiles of hybridized DE and PSSW2 modes, combined with the optical sensitivity of the BLS signal to the upper side of the CCFA or Co₂FeAl film, due to a limited probing depth.

VI. ACKNOWLEDGMENT

The project was financially supported by the Research Unit 559 “*New materials with high spin polarization*” funded by the Deutsche Forschungsgemeinschaft and by the Stiftung Rheinland-Pfalz für Innovation.

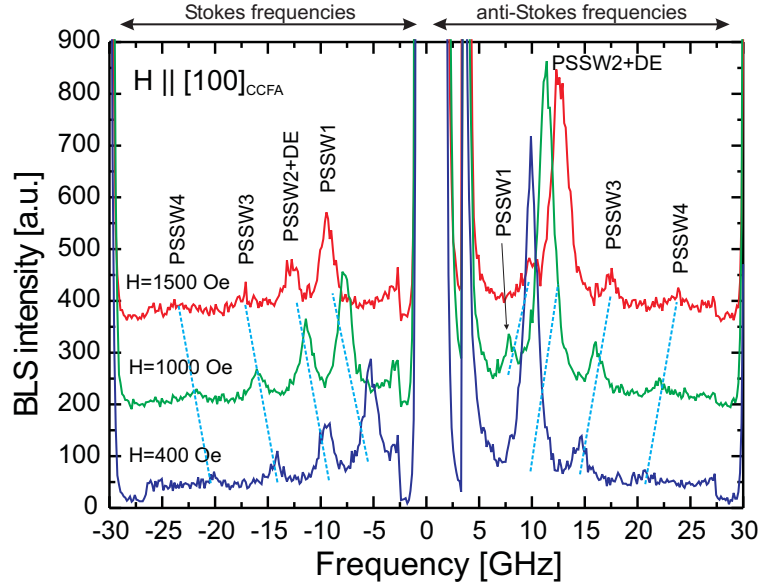


FIG. 1: (color online) Selected BLS spectra measured on the CCFA(80 nm) film in an external magnetic field of $H = 400, 1000$ and 1500 Oe. Negative frequencies are related to Stokes processes (creation of magnons), whereas positive frequencies are related to anti-Stokes processes (annihilation of magnons). The dashed lines are guides to the eye.

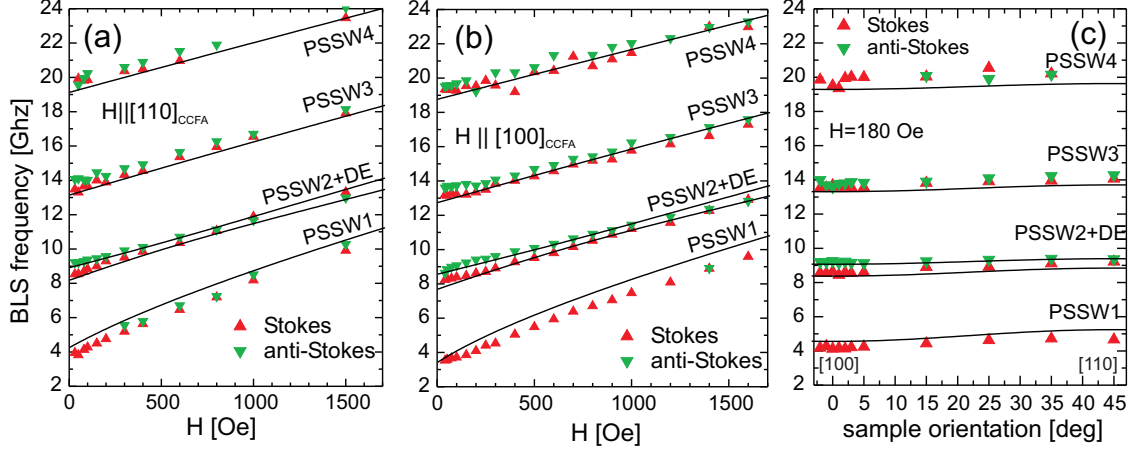


FIG. 2: (color online) (symbols) (a)(b) Dependence of the experimental BLS frequencies on the external magnetic field for H applied along the $[110]_{\text{CCFA}}$ (a) and the $[100]_{\text{CCFA}}$ axis (b). (c) Dependence of the BLS frequencies on the sample orientation, i.e. the angle between the $[100]_{\text{CCFA}}$ axis and the in-plane applied magnetic field. Triangles-up (down) refer to Stokes (anti-Stokes) frequencies of the BLS spectra. In all three panels, solid lines are the calculated spin-wave frequencies in CCFA(80 nm) using the exchange constant $A = 0.48 \mu\text{erg}/\text{cm}$, saturation magnetization $M_S = 520 \text{ emu}/\text{cm}^3$, Landé g -factor $g = 1.9$, transferred wave vector $q_{\parallel} = 1.67 \cdot 10^5 \text{ cm}^{-1}$ and cubic volume anisotropy $K_1 = -20 \text{ kerg}/\text{cm}^3$.

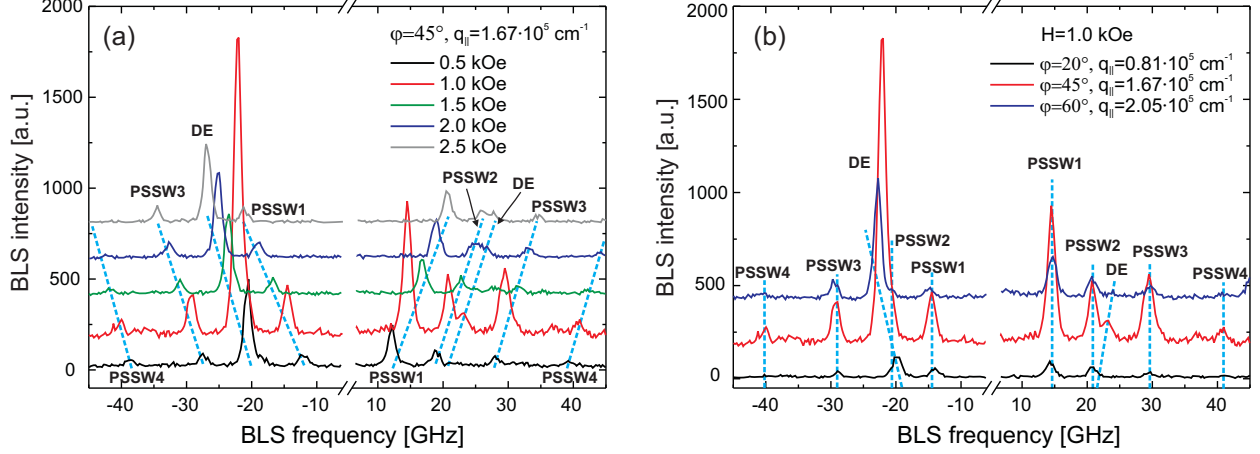


FIG. 3: (color online) (a) BLS spectra of Co_2FeAl recorded at a transferred wave vector $q_{\parallel} = 1.67 \cdot 10^5 \text{ cm}^{-1}$ and different magnetic fields. The change of peak positions upon the variation of the magnetic field reveals the magnonic origin of the peaks. (b) BLS spectra of Co_2FeAl recorded in an external applied field H of 1 kOe and different incidence angles φ . In (a-b), the dashed lines are guides to the eye. The DE mode exhibits a strong dependence on φ , whereas the frequency of the PSSW modes does not significantly change with φ . A clear distinction between the DE and PSSW modes thus becomes possible. For the assignment of the standing spin wave peaks to different modes see the text.

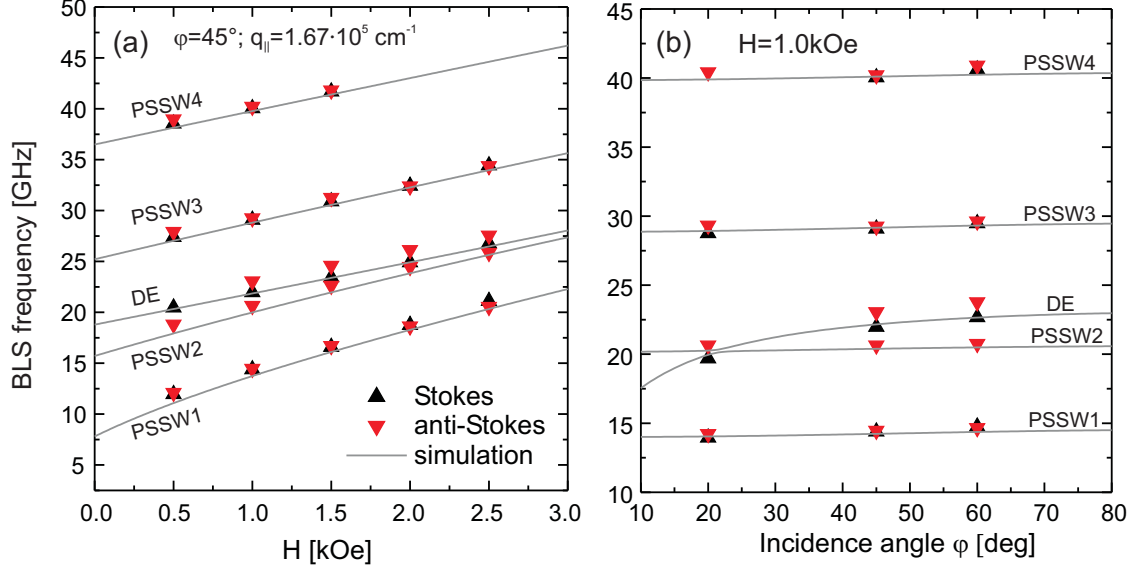


FIG. 4: (color online) (symbols) Experimental BLS frequencies of Co₂FeAl, corresponding to the peak positions in the BLS spectra presented in Fig. 3(a) and (b). (solid lines) Simulations for the exchange constant $A = 1.55 \mu\text{erg}/\text{cm}$, saturation magnetization $M_S = 1027 \text{ emu}/\text{cm}^3$ and Landé g -factor $g = 2.1$. (a) shows the dependence of BLS frequencies on the external magnetic field, whereas (b) demonstrates the dependence of BLS frequencies on the angle of incidence φ .

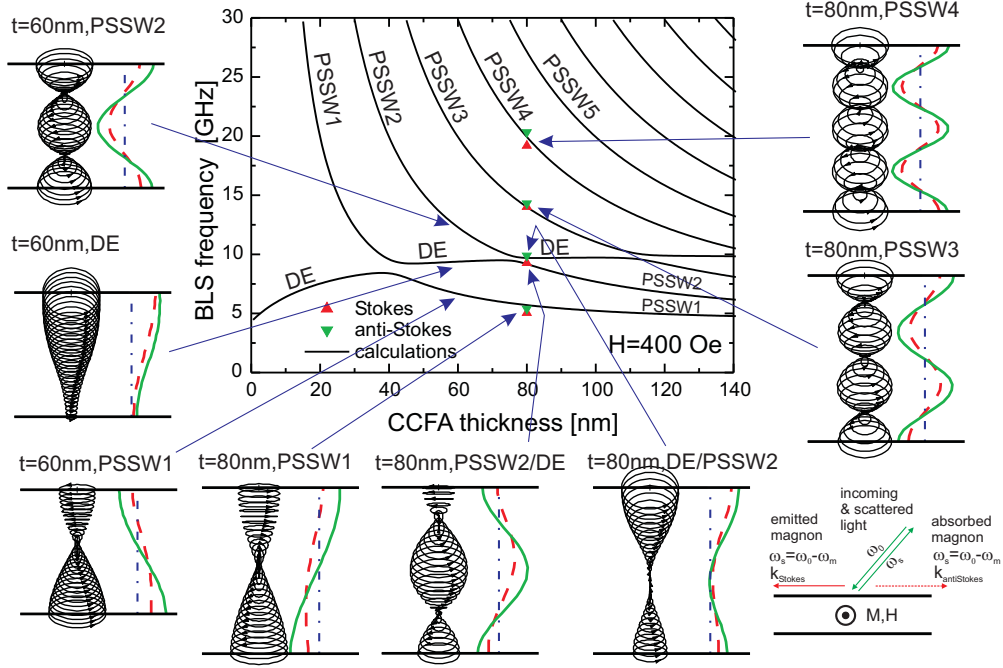


FIG. 5: (color online) Calculated dependence of spin-wave frequencies on the thickness of the CCFA film for $H = 400$ Oe, $H \parallel [100]_{\text{CCFA}}$ and a transferred spinwave wavevector $q_{\parallel} = 1.67 \cdot 10^5 \text{ cm}^{-1}$. Symbols (solid line) represent experimental data (simulations). The parameters used in the simulations are the same as in Fig. 2. The graph is surrounded by calculated profiles of spin-wave modes over the film thickness for $t = 60$ and 80 nm. The left part of each profile image shows the trajectory of magnetization when looking onto the magnetization vector. The right part shows the corresponding profile of the amplitude of the dynamic magnetization in the out-of plane (red dashed line) and the in-plane (green solid line) directions, respectively. The sketch in the bottom-right corner shows the used geometry.

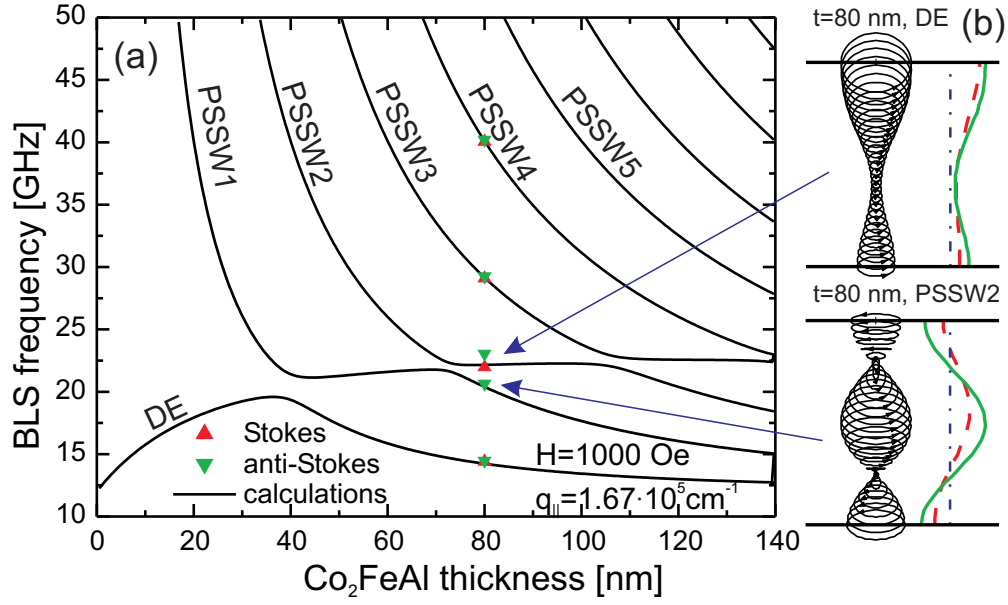


FIG. 6: (color online) (a) Calculated dependence of spin-wave frequencies on the thickness of the Co₂FeAl film for $H = 1000$ Oe and for spinwave's transferred wavevector $q_{||} = 1.67 \cdot 10^5 \text{ cm}^{-1}$. Symbols (solid line) represent experimental data (simulations). The parameters used in the simulations are the same as in Fig. 4. (b) Profiles of dynamic magnetization for the DE and PSSW2 modes, calculated for $t = 80$ nm.

-
- [1] Fecher GH, Kandpal HC, Wurmehl S, Felser C, Schönhense G 2006 *J. Appl. Phys.* **99**(8) 08J106
- [2] Ramsteiner M, Brandt O, Flissikowski T, Grahn HT, Hashimoto M, Herfort J, Kostial H 2008 *Phys. Rev. B* **78**(12) 121303
- [3] Felser C, Heitkamp B, Kronast F, Schmitz D, Cramm S, Dürr HA, Elmers H, Fecher GH, Wurmehl S, Block T, Valdaitsev D, Nepijko SA, Gloskovskii A, Jakob G, Schönhense G, Eberhardt W 2003 *J. Phys. Condens. Matter* **15** 7019
- [4] Hirohata A, Kurebayashi H, Okamura S, Tezuka N, Inomata K 2005 *IEEE Trans. Mag.* **41** 2802
- [5] Conca A, Jourdan M, Herbort C, Adrian H 2007 *J. Cryst. Growth* **299** 299
- [6] Wurmehl S, Alves MCM, Morais J, Ksenofontov V, Teixeira SR, Machado G, Fecher GH, Felser C 2007 *J. Phys. D: Appl. Phys.* **40**(6) 1524
- [7] Jourdan M, Conca A, Herbort C, Kallmayer M, Elmers HJ, Adrian H 2007 *J. Appl. Phys.* **102**(9) 093710
- [8] Ksenofontov V, Herbort C, Jourdan M, Felser C 2008 *Appl. Phys. Lett.* **92** 262501
- [9] Miura Y, Nagao K, Shirai M 2004 *Phys. Rev. B* **69** 144413
- [10] Antonov VN, Durr HA, Kucherenko Y, Bekenov LV, Yaresko AN 2005 *Phys. Rev. B* **72** 054441
- [11] Wurmehl S, Fecher GH, Kroth K, Kronast F, Dürr HA, Takeda Y, Saitoh Y, Kobayashi K, Lin HJ, Schönhense G, Felser C 2006 *J. Phys. D: Appl. Phys.* **39** 803
- [12] Inomata K, Okamura S, Miyazaki A, Kikuchi M, Tezuka N, Wojcik M, Jedryka E 2006 *J. Phys. D: Appl. Phys.* **39** 816
- [13] Galanakis I 2002 *J. Phys. Condens. Matter* **14** 6329
- [14] Cinchetti M, Wüstenberg JP, Albaneda MS, Steeb F, Conca A, Jourdan M, Aeschlimann M 2007 *J. Phys. D: Appl. Phys.* **40**(6) 1544–1547
- [15] Kelekar R, Clemens BM 2005 *Appl. Phys. Lett.* **86** 232501
- [16] Marukame T, Ishikawa T, Hakamata S, Matsuda Ki, Uemura T, Yamamoto M 2007 *Appl. Phys. Lett.* **90**(1) 012508
- [17] Marukame T, Ishikawa T, Hakamata S, Matsuda KI, Uemura T, Yamamoto M 2007 *IEEE Trans. Mag.* **43**(6) 2782

- [18] Hirohata A, Kurebayashi H, Okamura S, Kikuchi M, Masaki T, Nozaki T, Tezuka N, Inomata K 2005 *J. Appl. Phys.* **97** 103714
- [19] Hirohata A, Kurebayashi H, Okamura S, Masaki T, Nozaki T, Kikuchi M, Tezuka N, Inomata K, Claydon JS, Xu YB 2005 *J. Appl. Phys.* **97** 10C308
- [20] Tezuka N, Okamura S, Miyazaki A, Kikuchi M, Inomata K 2006 *J. Appl. Phys.* **99** 08T314
- [21] Takahashi YK, Ohkubo T, Hono K, Okamura S, Tezuka N, Inomata K 2008 *J. Magn. Magn. Mater.* **313** 378
- [22] Kandpal HC, Fecher GH, Felser C 2007 *J. Phys. D: Appl. Phys.* **40** 1507
- [23] Hamrle J, Blomeier S, Gaier O, Hillebrands B, Schäfer R, Jourdan M 2006 *J. Appl. Phys.* **100** 103904
- [24] Buschow KHJ, van Engen PG, Jongebreur R 1983 *J. Magn. Magn. Mater.* **38** 1
- [25] Mock R, Hillebrands B, Sandercock R 1987 *J. Phys. E: Sci. Instrum.* **20** 656
- [26] Hillebrands B 1999 *Rev. Scien. Instr.* **70** 1589
- [27] Hillebrands B. Brillouin light scattering spectroscopy. In: Zhu Y, editor. *Modern Techniques for Characterizing Magnetic Materials*, Kluwer Academic Publishers; 2005.
- [28] Hillebrands B 1990 *Phys. Rev. B* **41** 530
- [29] Pauthenet R 1982 *J. Appl. Phys.* **53**(11) 8187
- [30] Shirane G, Minkiewicz VJ, Nathans R 1968 *J. Appl. Phys.* **39**(2) 383
- [31] Liu X, Steiner MM, Sooryakumar R, Prinz GA, Farrow RFC, Harp G 1996 *Phys. Rev. B* **53** 12166
- [32] Graham CD 1958 *Phys. Rev.* **112**(4) 1117
- [33] Gaier O, Hamrle J, Hermsdoerfer SJ, Schultheiß H, Hillebrands B, Sakuraba Y, Oogane M, Ando Y 2008 *J. Appl. Phys.* **103**(10) 103910
- [34] Liu Y, Shelford LR, Kruglyak VV, Hicken RJ, Sakuraba Y, Oogane M, Ando Y, Miyazaki T 2007 *J. Appl. Phys.* **101**(9) 09C106
- [35] Stöhr J, Siegmann HC. *Magnetism. From fundamentals to nanoscale dynamics*. Springer; 2006
- [36] Kalinikos BA, Slavin AN 1986 *J. Phys. C* **19** 7013
- [37] Hamrle J, Ferré J, Nývlt M, Višňovský v 2002 *Phys. Rev. B* **66**(22) 224423
- [38] Buchmeier M, Dassow H, Bürgler DE, Schneider CM 2007 *Phys. Rev. B* **75**(18) 184436
- [39] The dynamic magnetization is the difference between the static magnetization \vec{M}_0 and its

instantaneous value $\vec{M}(t)$: $\vec{m}(t) = \vec{M}(t) - \vec{M}_0$.